ELSEVIER

Journal of Photochemistry and Photobiology A: Chemistry 107 (1997) 9–19

Journal of PHOTOCHEMISTRY AND PHOTOBIOLOGY A: CHEMISTRY

Identification of nascent products formed in the laser photolysis of CH_3OCl and HOCl at 308 nm and around 235 nm. Total Cl-atom quantum yields and the state and velocity distributions of $Cl(^2P_j)$

R.N. Schindler *, M. Liesner, S. Schmidt, U. Kirchner, Th. Benter

Institut für Physikalische Chemie, Christian-Albrechts-Universität zu Kiel, Ludewig-Meyn Str. 8, D-24098 Kiel, Germany

Received 30 November 1995; accepted 25 November 1996

Abstract

Nascent products formed in the laser photolysis of the two hypochlorites CH_3OCl and HOCl at wavelengths close to the maxima in their absorption spectra have been determined by resonantly enhanced multiphoton ionisation (REMPI) using a time-of-flight (TOF) mass analyser. Cl-atoms in the states $^2P_{3/2}$ and $^2P_{1/2}$ were found to be the predominant photodissociation products for both hypochlorites. In the case of HOCl, the nascent OH was also recorded with rotational resolution. Formation of other possible photofragments from CH_3OCl i.e. HCl, CH_3 and ClO was clearly excluded to $<10^{-2}$ and $<10^{-3}$, respectively.

The absolute quantum yields for Cl-atom production in the photolysis at the atmospherically relevant wavelength of $\lambda = 308$ nm were found to be $\Phi = 0.95 \pm 0.05$ and $\Phi = 1.00 \pm 0.05$ for CH_3OCl and HOCl, respectively. Relative spin-orbit state population of the nascent chlorine (^2P_j) atoms varied strongly with photolysis wavelength.

The kinetic energy released to the Cl-atoms in the photolysis at two wavelengths was determined for CH_3OCl and HOCl for the first time. In the photolysis at $\lambda = 308$ nm, Cl-atoms are formed with E_{trans} of about 1 eV. The atmospheric implications of this finding are briefly outlined. © 1997 Elsevier Science S.A.

Keywords: Laser photolysis; CH_3OCl; HOCl quantum yields; State distribution; Velocity distribution

1. Introduction

The hypochlorites HOCl and CH_3OCl are considered to be important atmospheric Cl-reservoir compounds, which upon photolysis liberate Cl-atoms. Laboratory experiments have established [1–10] that HOCl and CH_3OCl are effectively formed through the homogeneous gas phase radical reactions (Eqs. (1) and (2)), respectively,

$$HO_2 + ClO \rightarrow HOCl + O_2 \quad (1)$$

$$CH_3O_2 + ClO \rightarrow CH_3OCl + O_2 \quad (2)$$

Formation of hypochlorites in the atmosphere can be attributed to the same processes. In periods of highly disturbed stratospheric ozone chemistry [11], heterogeneous reactions may contribute to ROCl formation to a significant extent.

Recent UV/VIS-spectroscopic studies on molecules ROCl, with R being H, CH_3, C_2H_5, *iso*-C_3H_7 or *tert*-C_4H_9 [12–14] have revealed a high degree of similarity in the photoabsorption patterns of ROCl molecules between 220 and 400 nm. Absorption cross sections σ are reported for CH_3OCl and HOCl in the 10^{-19} cm^2 per molecule range. For HOCl the experimental absorption data are in good agreement with results of new potential energy surface calculations for electronic ground and excited states obtained by ab initio molecular orbital configuration interaction methods [15,16]. The experimental and theoretical findings thus support the notion that ROCl molecules, generated in the stratosphere, may contribute to ozone depletion through photodissociation.

The dissociation process for HOCl may be written as

$$HOCl(1^1A') + h\nu \rightarrow OH(^2\Pi_i) + Cl(^2P_j) \quad (3)$$

The excited states which correlate with the dissociation process (Eq. (3)) in the wavelength range 220–400 nm, are labelled $1^1A''$ and $2^1A'$. This pair of states results from single photon excitations $(\pi_{OCl}) \rightarrow (\sigma^*_{OCl})$ and $(\pi^*_{OCl}) \rightarrow (\sigma^*_{OCl})$ to the linear $1^1\Pi$ conformer. Following the arguments presented in theoretical studies [15,16], photodissociation of HOCl should lead to OH fragment rotational state distributions which depend on the excited state involved.

* Corresponding author. Tel: +49 431 880 2815/16. Fax: +49 431 880 2530.

PII S1010-6030(96)04583-2

Such fragment population distributions for OH and OD following photolysis of HOCl and DOCl, respectively, at 248 nm and 266 nm i.e. virtually in the same electronic transition have been investigated by Frey and co-workers [17–19]. Similar distributions were obtained at the both wavelengths. The $^2\Pi_{3/2}$ state was found to be more populated than the $^2\Pi_{1/2}$ state. No theoretical predictions are available on changes in spin-orbit coupling upon variation of photolysis wavelengths. The relative spin-orbit state population for nascent chlorine atoms from HOCl photolysis at two neighbouring wavelengths has been reported in Ref. [20]. A preference for production of ground-state $Cl(^2P_{3/2})$ was concluded from the obtained ratio $Cl^*/Cl = 0.30 \pm 0.07$.

The kinetic energy released into the fragments of hypochlorite photodissociation has been investigated by Thelen et al. [21] who have studied the *tert*-butyl hypochlorite photochemistry at 248 nm and 308 nm in a molecular beam by photofragment translational spectroscopy. Bell et al. [20] registered Cl^+ arrival time spectra to extract kinetic energy estimations from HOCl photolysis experiments.

Despite of all these efforts the photodissociation dynamics of the triatomic HOCl molecule can hardly be considered as well understood. As a matter of fact, even the absorption properties of HOCl in the near UV-region have until recently been the subject of some debate. In the same way as HOCl, also CH_3OCl might act as Cl-reservoir compound in the atmosphere. On the photochemistry of CH_3OCl and its dynamics virtually nothing is known.

In the present contribution, results are described for the first time on the identification of nascent products formed in the laser photolysis of CH_3OCl. Results from experiments with HOCl are included. Photolysis and photoionisation of the nascent photofragments was carried out in the ion source of a TOF mass spectrometer. Products were probed at a time ≤ 40 ns after photolysis, and thus diffusion out of the reaction volume as well as quenching may be excluded. Ionisation was obtained in multiphoton absorption processes. In CH_3OCl photolysis, nascent $Cl(^2P_{3/2})$ and $Cl^*(^2P_{1/2})$ were identified. Formation of CH_3 and ClO as well as of HCl was clearly excluded. In HOCl photolysis, $Cl(^2P_{3/2})$, $Cl^*(^2P_{1/2})$ and $OH(^2\Pi_{3/2})$ were identified. Formation of ClO and HCl was again excluded. Total quantum yields for Cl-production were determined in the photolysis of CH_3OCl and of HOCl. Finally, also the kinetic energy released to the photofragment $Cl(^2P_j)$ was determined with high resolution. Photolysis of Cl_2 and of NOCl and ClO radicals, the latter generated in the flow system outside of the mass spectrometer, were used as standards for internal calibrations and for the determination of spin orbit distributions, which varied strongly with photolysis wavelength and for the energy released to the product Cl atom.

2. Experimental

All experiments were carried out under flow conditions employing an UV/VIS absorption cell of 42-cm length coupled to a commercial Bruker TOF1 mass spectrometer (MS) via a pulsed metal-free shutter and a differential pumping stage. The two stage, grid-free ion source has been adapted to run in two different modes. A field strength in the extraction region of the ion source of $E_{est} \approx 600$ V cm^{-1} was used to collect the nascent photofragments for quantum yield determinations, a field strength of $E_{est} \approx 90$ V cm^{-1} was employed to determine recoil velocities (see Appendix). The absorption cell was equipped with a White optics system providing an effective path length of 3.36 m. In situ spectroscopic analysis of gas mixtures prior to photolysis in the ion source was carried out using a Jobin-Yvon monochromator type HR250 with a 300 line/mm grating equipped with a diode array arrangement for wavelength coverage in the range 230 nm $< \lambda < 400$ nm.

The reflectron type TOF-MS was equipped with a combined electron-impact/photoionisation source. A conven-

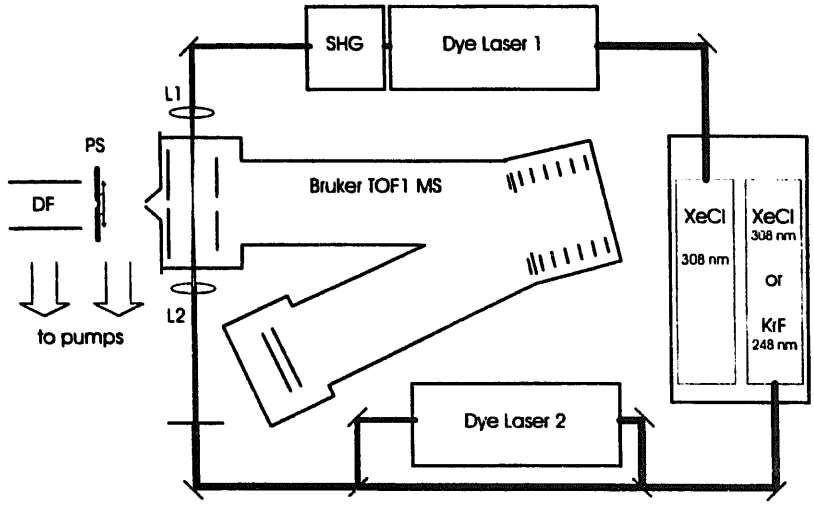

Fig. 1. Experimental set-up: Bruker TOF-mass spectrometer with Reflectron. The two excimer lasers were discharged simultaneously with one thyratron. Polarization of excimer laser radiation at $\lambda = 308$ nm was reached by passing the light over served mirrors and/or through a polarizer. DF: flow tube, PS: pulsed shutter, L1, L2: focusing lenses, SHG: second harmonic generator.

tional pump-probe set-up as shown schematically in Fig. 1 was used for mass selected REMPI analysis of the nascent neutral photofragments. The photolysis/photoionisation light sources used consisted of a Lambda Physik excimer laser/dye laser combination. The two discharge tubes of the EMG150 excimer laser were operated either with one tube at $\lambda = 248$ nm (KrF*) and one at $\lambda = 308$ nm (XeCl*) or with both tubes at $\lambda = 308$ nm. One of the beams could be strongly attenuated to be used directly for photolysis at $\lambda = 248$ nm or at $\lambda = 308$ nm, the second beam pumped a FL3002 dye laser to generate tuneable radiation for selective detection. In later experiments also two dye lasers were used. Dye laser emission was also employed for photolysis. The probe wavelength ranges covered were 230 nm $< \lambda <$ 250 nm using frequency doubled Coumarin 102 radiation and 330 nm $< \lambda <$ 350 nm obtained directly from *para*-terphenyl. Laser pulse energies were measured with a calibrated pyroelectric detector (Gentec, ED200). Typical pulse energies were 0.5 mJ for the frequency doubled radiation and up to 2 mJ for *para*-terphenyl. Pump and probe laser beams were focused with spherical lenses of 10 cm focal length and directed through the ion source perpendicular to the molecular beam but in opposite directions from each other. To obtain variable time delays between pump and probe beams, it was necessary to insert or remove capacitors of the excimer discharge system since both tubes were discharged simultaneously with one thyratron. In two-colour experiments the probe pulse was delayed for 40 ns relatively to the 308 nm photolysis pulse.

Flow rates were chosen such that residence times of gases in the absorption cell were <3 s at pressures 5–40 mbar. Absolute concentrations of HOCl and CH_3OCl were obtained from UV absorption measurements using recently determined cross sections [12,13]. The gas flow entering the ion source for photolysis was further analysed by electron impact (EI) ionisation.

Gaseous HOCl samples were obtained by bubbling helium through aqueous <0.5 M HOCl solutions held at $T = 0$ °C. The solutions were freshly prepared as described in [22]. The water content in the gaseous sample was controlled with a cold trap held at $T < -10$ °C. The trap effluent was added to the main He carrier gas flow into the UV absorption cell [22]. The gas flow contained also negligible amounts of Cl_2 as determined by MS analysis and $\leq 1\%$ Cl_2O as obtained from absorption measurements. CH_3OCl was prepared as described in [12] in analogy to the synthesis given by Sandmeyer [23]. CH_3OCl was purified by repeated trap to trap distillations and stored as liquid in small glass containers held at dry ice temperature. CH_3OCl was added as neat sample to the main gas flow. It contained 1% CH_3OH as impurity, which had been measured by FTIR. Molecular chlorine was not detectable. A mixture of 10% Cl_2 (>99.8) in helium (Messer Griesheim) was used for calibration purposes. NOCl was available as liquid (Aldrich) and was stored as gaseous sample in a blackened glass bulb.

Thermalized ClO radicals were generated in a side arm of the UV cell at pressures <20 mbar through the reaction of O atoms with OClO. The main processes are shown in Eqs. (4)–(6):

$$OClO + O \rightarrow ClO + O_2 \quad (4)$$

$$ClO + O \rightarrow Cl + O_2 \quad (5)$$

$$Cl + OClO \rightarrow 2ClO \quad (6)$$

OClO was prepared in situ by carefully adjusting the flow of 10% Cl_2 in He through a tube with glass beads covered with moist $NaClO_2$ (Hoechst). The purity of chlorine dioxide produced in this way was routinely monitored with EI ionisation and was always $>99\%$. Absolute [ClO] and [OClO] were calculated from UV absorption measurements [11] and recorded continuously.

3. Results

3.1. Identification of nascent products

Photolysis experiments were carried out at $\lambda = 308$ nm and 248 nm using the attenuated beams of the excimer lasers and in the wavelength range from 232 nm $< \lambda <$ 241 nm using the output of the frequency doubled dye laser. In the latter investigations, which are single laser experiments, the dye laser was used for photolysis and subsequent ionisation of the nascent products.

The dissociation channels (Eqs. (a)–(d)) were considered. Employing radiation from the KrF* – laser or the frequency doubled dye-laser they are thermodynamically allowed, provided the photofragments are formed in their electronic ground state: In (Eq. c) the O-atoms can also be formed in the state ^1D.

$$CH_3OCl(HOCl) + h\nu \rightarrow CH_3O(HO) + Cl \quad (a)$$

$$\rightarrow CH_3(H) + ClO \quad (b)$$

$$\rightarrow CH_3Cl(HCl) + O \quad (c)$$

$$\rightarrow HCl + CH_2O \quad (d)$$

In all photolysis experiments with CH_3OCl and with HOCl, Cl atoms in the doublet states $^2P_{3/2}$ (Cl) and $^2P_{1/2}$ (Cl*) were detected. In Fig. 2 are reproduced two of the twelve (2+1) REMPI lines for Cl-atoms located in the wavelength range 232 nm $< \lambda <$ 238 nm. Their identification was established through known (2+1) REMPI processes for neutral ground state Cl-atoms [24,25]. To monitor and to evaluate quantitatively the relative population in the two spin orbit states the transitions $4p^2D_{3/2} \leftarrow 3p^2P_{3/2}$ for Cl at $\lambda = 235.336$ nm and $4p^2D_{3/2} \leftarrow 3p^2P_{1/2}$ for Cl* at $\lambda = 237.808$ nm were used.

To test whether the formal intensity law is properly obeyed in our experiments and to determine the order of the multiphoton processes studied, the power dependence for Cl^+ – ion signals at $\lambda = 235.336$ nm was recorded as obtained in the photolysis of CH_3OCl and HOCl. This was done in

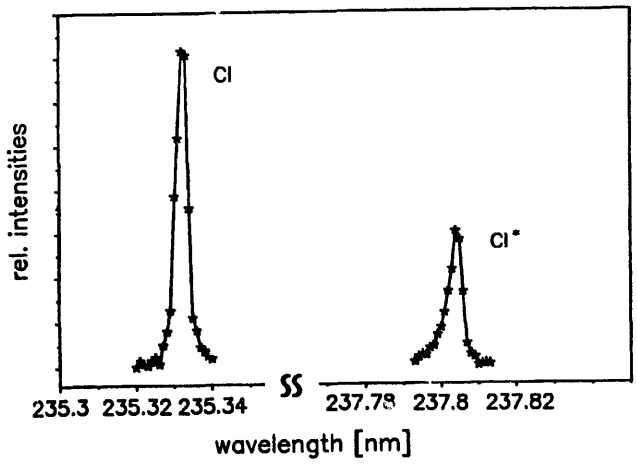

Fig. 2. REMPI signals of $Cl(^2P_{3/2})$ atoms at $\lambda = 237.33$ and $Cl^*(^2P_{1/2})$ atoms at $\lambda = 237.08$ nm as generated in the photolysis in single laser experiments.

single laser experiments by variation of the laser discharge high voltage. The recorded signal intensities corresponded to the integrated area of the resonance lines. With CH_3OCl, a linear dependence with a slope of 3.79 ± 0.37 was obtained, with HOCl, a slope of 3.88 ± 0.09 resulted. The dependencies are plotted on logarithmic axes in Fig. 3. Within experimental error the slopes are identical. The power dependencies are taken as evidence for a four photon process. Thus the Cl^+ – ions detected in CH_3OCl photolysis experiments must originate from Cl-atoms generated photolytically in the ion source through a one-photon absorption process, followed by absorption of three photons for the (2+1) REMPI probe. Fragmentation of photoions, e.g. of CH_3OCl^+ would not show the observed resonant wavelength behaviour for Cl-atoms. Ion fragmentation to yield neutral Cl, followed by a (2+1) REMPI process would be indicated by a higher power dependence. Since molecular collisions in the ion source can be excluded, the observed Cl^+ signals represent nascent Cl radicals generated through photolysis. The same arguments hold for the Cl^+ – ions recorded in the photolysis of HOCl.

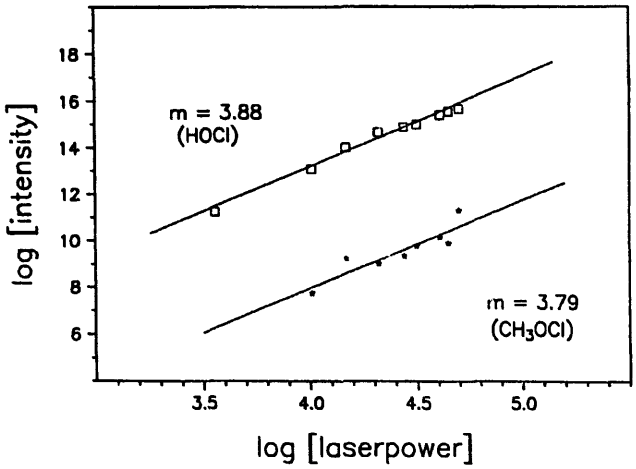

Fig. 3. Power dependencies for the $Cl(^2P_{3/2})$ atom REMPI signals generated in the photolysis of CH_3OCl and HOCl, respectively, in single laser experiments. The laser power was ≤400 μJ per pulse.

No REMPI signal was obtained for the dissociation fragment CH_3O. The reason for this failure is not known. Our attempts to detect this radical by REMPI had also failed in experiments, in which CH_3O radicals had been generated in flow experiments in concentrations up to 1×10^{13} molecule per cm^3 [26]. Presumably the REMPI sensitivity for this species is very low. With the dye-laser beam being strongly focused, ion signals at $m/e = 31$ (CH_3O^+) were observed in the wavelength range between 230 and 255 nm. However, the wavelength dependence of this signal was identical with the dependencies of photoion signals recorded at $m/e = 15$ (CH_3^+) and $m/e = 66$ ($CH_3O^{35}Cl^+$). Thus, this signal is to be assigned to a fragment of the parent ion molecule CH_3OCl^+ and is not due to the photolytically generated species CH_3O.

Formation of other possible products in the photolysis of CH_3OCl, such as CH_3, ClO or HCl was clearly excluded. If formed, they would have been identified by REMPI with high sensitivity under conditions as compiled in Table 1. CH_3 radicals, if present can be identified at $m/e = 15$ using the strong $3p^2A_2'' \leftarrow 2p/\tilde{X}^2A_2''$ transition at the one-photon wavelength of $\lambda = 333.33$ nm [27]. The detection limit for CH_3 radicals has been estimated from experiments in which CH_3O_2 was photolysed at 248 nm [26] and the CH_3 formed was detected by REMPI. In the CH_3OCl photolysis under identical conditions for the photolysis laser and the probe laser no ion signal at $m/e = 15$ was detectable. Taking into account the different concentrations of CH_3OCl and CH_3O_2 being introduced into the ion source and their absorption cross sections at 248 nm the upper limit for CH_3 quantum yield in the CH_3OCl photolysis can be given as $\Phi_{248nm}^{CH_3} < 0.01$. For ClO and HCl the REMPI sensitivity was obtained from experiments under flow conditions. Again upper limits for $\Phi_{248\ nm}^{HCl} < 0.01$ and for $\Phi_{248\ nm}^{ClO} < 0.001$ were inferred from the experiments.

In contrast to the experiments with CH_3OCl, in the photolysis of HOCl the corresponding photofragment OH was detected by photoionisation. The observed partially resolved rotation spectrum for the fragment OH, as obtained in the photolysis at $\lambda = 244$ nm, recorded at the ion mass 17 is shown in Fig. 4. The REMPI spectrum of OH was also registered in the photolysis at $\lambda = 308$ nm (see below). Ionisation occurred in a (2+1) process using the $D^2\Sigma^-$ Rydberg manifold as intermediate state [28,29]. The assignment was carried out with the spectroscopic constants taken from de Beer [29] and Dieke [30]. Absorptions observed at 244.2 nm

Table 1
Transitions used for (2+1)REMPI detection of photolysis products

Species	One-photon wavelength (nm)	Transition	Ref.
ClO	341.74	$C^2\Sigma^- \leftarrow X^2\Pi$	[49]
HCl	241.1	$F^1D \leftarrow X^2\Sigma^+$	[50]
CH_3	333.32	$3p^2A''_2 \leftarrow 2pX^2A''_2$	[27]
OH	244.2	$D^2\Sigma^- \leftarrow X^2\Pi$	[28,29]

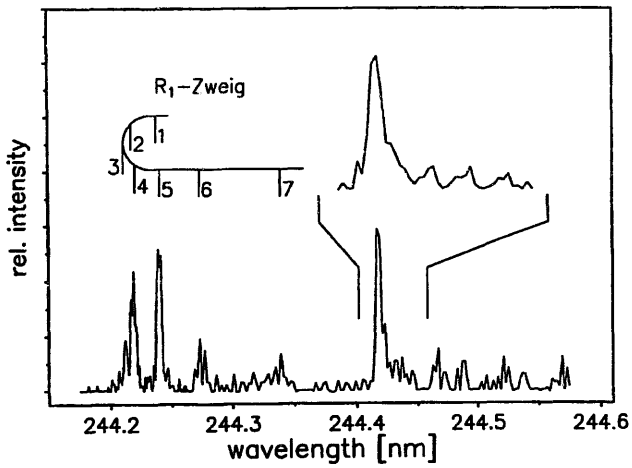

Fig. 4. (2+1) REMPI spectrum of the $D^2\Sigma(v'=0) \leftarrow X^2\Pi(v''=0)$ transition for OH radicals generated in the photolysis of HOCl at 244.1 nm $< \lambda <$ 244.6 nm in a single laser experiment and recorded at ion mass 17.

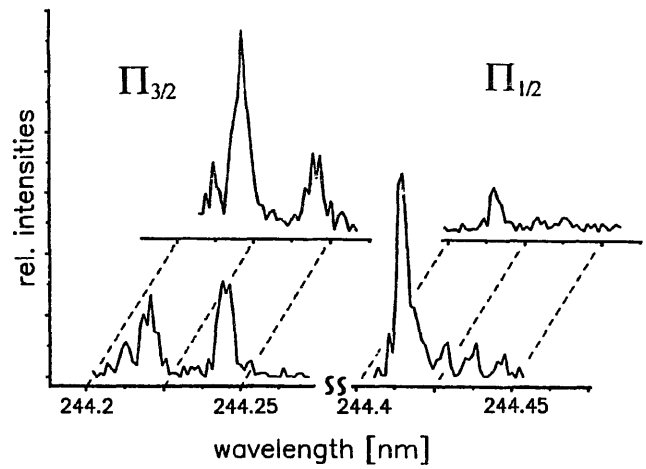

Fig. 5. Selected sections from OH radical REMPI spectra as obtained in the HOCl photolysis at $\lambda = 308$ nm (upper trace) and in a single laser photolysis/photoionization experiment (lower trace). For details cf. Fig. 4.

$< \lambda <$ 244.25 nm are due to the R_1-branch, corresponding to the $^2\Pi_{3/2}$ ground state of OH [29,30]. At the longer wavelength, i.e. 244.4 nm $< \lambda <$ 244.45 nm, no unambiguous interpretation was possible. The low wavelength resolution of 0.7 cm^{-1} available in the present laser experiments was too poor to resolve overlapping Q_1 and R_2 branches. If the structure were predominantly due to the R_2-branch, this would indicate a preference for a dissociation into the excited $OH(^2\Pi_{1/2})$ state at the shorter photolysis wavelength. Alternatively, a change in the population of the two different Λ-doublet states with increasing photolysis wavelength could be indicated, because Q- and R-branches are probing different Λ-doublet levels due to their symmetry properties [31].

In experiments with HOCl the same upper limits were obtained for HCl and ClO formation as for CH_3OCl. The results for HOCl are in good agreement with values reported in earlier studies [32].

3.2. *Relative spin-orbit state distributions and total quantum yields*

Ab initio model calculations have shown that the electronically exited states of HOCl are strongly repulsive in the O-Cl coordinate [15,16]. This implies that photodissociation should be a direct process leading to HO + Cl photofragment formation with presumably unity quantum yield. Ab initio model calculations for CH_3OCl are not available. Since the general feature of the UV/VIS absorption spectra of CH_3OCl and HOCl exhibit a high similarity [12] it is tacitly assumed that the photodecomposition of CH_3OCl will also occur along the repulsive O-Cl coordinate. The ground state HOCl-($^1\Sigma^+$) molecule possesses a bent configuration with $\angle$ HOCl = 102.9° [33]. The electronically exited states $1^1A''$ and $2^1A'$ reached in the spectral range of interest for the present consideration are also slightly bent in the Franck-Condon region [15,34]. It has been argued that the excess energy available in the photodissociation process is hardly transmitted to the rotation of the OH fragment and that the rotational excitation of the OH photofragment will be low [15].

Unfortunately the obtained REMPI mass spectra for OH as recorded with the present set-up were of low intensity and of limited resolution only (see Fig. 4). Thus an analysis of the OH rotational population distribution was precluded from the present investigation. However, the OH radicals detected (cf. Fig. 5) in the photolysis of HOCl at $\lambda = 308$ nm and at $\lambda = 244$ nm showed a pronounced change in relative spin-orbit population. Whereas in the 308-nm photolysis the nascent $^2\Pi_{3/2}$-state signal appears of higher intensity than the $^2\Pi_{1/2}$ signal, this ratio is reversed in the photolysis at $\lambda = 244$ nm. No further conclusions shall be derived at present from this observation (see also above on uncertainties with respect to the assignment).

Due to the limited spectral resolution and the relatively low intensity of the OH ion signals no value on the quantum yield for OH formation in the photolysis of HOCl could be extracted from the present experiments. However, for Cl atoms generated in the photolysis of CH_3OCl and of HOCl new data became available on the wavelength dependence of nascent spin-orbit population ratios. Also the total quantum yields for Cl atom generation from CH_3OCl and HOCl photolysis at $\lambda = 308$ nm have been determined. For these evaluations the REMPI sensitivity of the mass spectrometer to Cl-atoms formed in the two spin-orbit states must be known. Such sensitivities have been reported by Barclay et al. [35] and by Tonokura et al. [36]. The former study was based on an investigation by Tiemann et al. [37]. These authors have photodissociated HCl at 193 nm in the pressures range 0.1–0.3 Torr using an ArF laser. The atomic fine structure transition $^2P_{1/2} - {}^2P_{3/2}$ in Cl-atoms at 882.35 cm^{-1} served as probe for the population of the two spin orbit states. Tiemann et al. [37] found populations of 67% Cl and 33% Cl*, in close agreement with values calculated from the statistical weights of the two fine structure levels. Barclay et al. [35] referenced these values to their photolysis results at the same wavelengths using (2+1) REMPI for Cl-detection. They

Table 2
Measured Cl*/Cl spin orbit population ratios in the photolysis at two wavelengths and the ratio for thermal Cl-atoms, calculated with an energy difference of 881 cm^{-1} between the two Cl levels using a Boltzmann distribution

Photolysis wavelength (nm)	CH_3OCl	HOCl	Cl_2
308	0.31 ± 0.02	0.035 ± 0.002	0.0068 ± 0.0004
235/237	1.45 ± 0.05	0.34 ± 0.02	0.95 ± 0.05
Thermal Cl-atoms	–	–	0.0073

showed that the signal from $Cl(^2P_{3/2})$ was 5.3 ± 0.5 times more intense than from $Cl^*(^2P_{1/2})$, thus yielding a REMPI detection sensitivity ratio of 2.7 ± 0.3. Tonokura et al. [36] calibrated REMPI sensitivities for the fine structure branching using data as obtained in VUV-LIF experiments and reported a value of 2.5 ± 0.1 for the sensitivity ratio. This latter value was adopted in the present study for the calculations of relative spin-orbit populations and of quantum yields.

In the photolysis of CH_3OCl, the probability P to generate $Cl^*(^2P_{1/2})$ relative to $Cl(^2P_{3/2})$ is found to be $P = 0.31 \pm 0.02$ at $\lambda = 308$ nm and $P = 1.45 \pm 0.05$ at $\lambda = 235$ nm. In the photolysis of HOCl these probabilities were $P = 0.035 \pm 0.02$ at $\lambda = 308$ nm and $P = 0.35 \pm 0.02$ at $\lambda = 235$ nm. This latter value is in good agreement with the only previously reported value by Bell et al. [20], who quoted for the relative spin-orbit state population a ratio of $P = 0.30 \pm 0.07$. For reference, in the present investigation also the relative spin-orbit population was determined for nascent $Cl(^2P)$ atoms generated in the photolysis of Cl_2 at $\lambda = 308$ nm. The value $P = (6.9 \pm 0.4) \times 10^{-3}$ found in the present study is in good agreement with $P = (9.5 \pm 1.8) \times 10^{-3}$ reported by Matsumi et al. [38]. For Cl atoms in thermal equilibrium at $T = 298$ K, a probability $P = 7.3 \times 10^{-3}$ would be expected. At both photolysis wavelengths sufficient energy is available to populate the $^2P_{1/2}$ state in the photolysis of CH_3OCl. The population inversion in photolysis at the shorter wavelength might thus be related to a change in the potential energy surface reached. All results on measured $Cl(^2P)$ spin-orbit population ratios from this investigation are compiled in Table 2.

In the evaluation of total Cl-atom quantum yields in the photolysis, molecular chlorine with $\Phi = 2$ for Cl-atom generation served as actinometer. The absorption cross sections σ in units cm^2 per molecule at $\lambda = 308$ nm as reported in literature, i.e. $\sigma\ (Cl_2) = 16 \times 10^{-20}$ [39], $\sigma\ (CH_3OCl) = 1.5 \times 10^{-20}$ [12] and $\sigma\ (HOCl) = 6.2 \times 10^{-20}$ [12] were used in the calculations. With the spin-orbit populations as given in Table 2 under identical photolysis conditions, i.e. identical laser intensity and absorbance by CH_3OCl and Cl_2 the total quantum yield for Cl production $\Phi = 0.95 \pm 0.05$ from CH_3OCl was determined in this study. From HOCl photolysis experiments under identical conditions a Cl-atom quantum yield of $\Phi = 1.00 \pm 0.05$ was obtained.

3.3. Velocity distribution of photogenerated $Cl(^2P)$ atoms

For a given experimental setting, the arrival time of a photofragment ion at the detector depends primarily on its mass and on its initial recoil energy along the drift tube axis, which the fragment receives in the photodissociation process. The site of photogragmentation and ionisation in the ion source is spatially sharply defined by the overlap region of the two collimated laser beams. The experimental ion peaks thus describe through their location fragment scalar properties of the forces acting in the dissociation process, as well as through their shape the vector properties of the products. The former reflects the partitioning of excess energy between relative translation and internal excitation, the latter the influence of the angular distribution on the velocity component distribution. For a direct dissociation process the angular distribution function for the fragment Cl generated by absorption of linearly polarized laser radiation [40–43] is given by:

$$\frac{dN(\theta)}{d\Omega} = \frac{1}{4}\Pi[1 + \beta P_2(\cos\theta)] \qquad (I)$$

where θ is the angle between recoil direction and the electric field vector of the laser radiation, β is the anisotropy parameter and P_2 is the second Legendre polynomial. The spatial anisotropy parameter lies between -1 and 2, which corresponds to the limits for a perpendicular and a parallel transition, respectively. Upon transformation of the angular distribution to the coordinates of the experiment [41,42] the TOF profiles can be expressed through the expression:

$$F(t) = \frac{1}{2}\Delta t\left[1 + \beta_{eff} P_2\left(\frac{t - t_0}{\Delta t}\right)\right] \text{ with}$$

$$\beta_{eff} = \beta P_2(\cos\alpha) \qquad (II)$$

where t_0 is the ion arrival time in the absence of fragment recoil energy and Δt is the maximum time lag from the photofragment kinetic energy release. The angle α, i.e. the orientation of the TOF axis to the polarisation of the photolysis laser, was zero in most of our experiments.

In Fig. 6(a) and (b) are displayed PF-TOF profiles for $Cl(^2P_{3/2})$ and for $Cl(^2P_{1/2})$, respectively, as obtained in the photolysis of CH_3OCl at $\lambda = 308$ nm. In Fig. 7 profiles for $Cl(^2P_{3/2})$ are given generated in the photolysis of NOCl at $\lambda = 355$ nm. The same profiles were also registered (but are not shown here) for $Cl(^2P_{3/2}, ^2P_{1/2})$ in the CH_3OCl photolysis at a wavelength of $\lambda = 235$ nm and $\lambda = 238$ nm, respectively. Equivalent profiles were obtained in HOCl photolysis experiments. However, besides exhibiting the expected reduced splitting, the records exhibited appreciable background scatter and shall not be presented here. A least-square fitting programme as outlined in Ref. [42] has been adopted to analyse the experimental results. Although several parameters become available from this fit, in the present paper only the evaluation of the recoil energy of the Cl fragment has been executed. More detailed results from investigations of photofragment velocity distributions in ROCl, ROBr

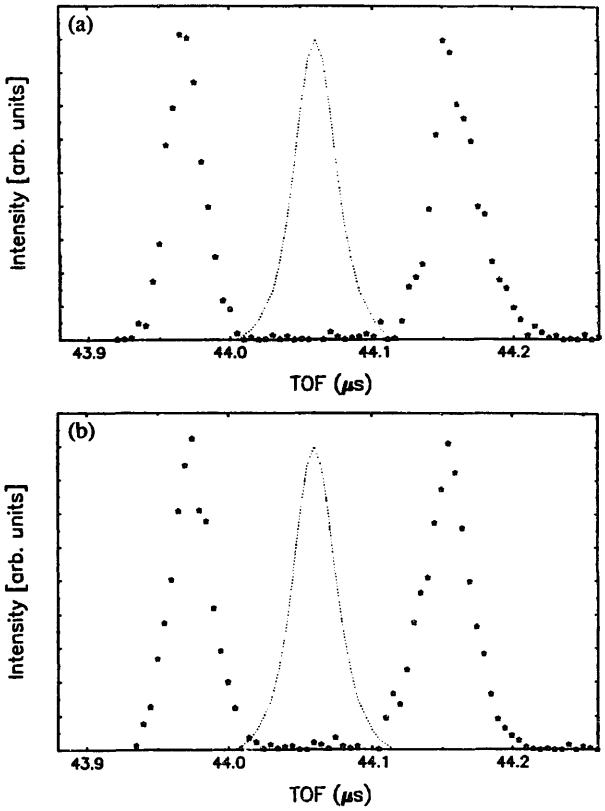

Fig. 6. REMPI PF-TOF profiles of $Cl(^2P_{3/2})$ atoms (a) and $Cl(^2P_{1/2})$ atoms (b) generated in the photolysis of CH_3OCl at $\lambda = 308$ nm. Asterisks are experimental data points. The dotted signal with a maximum around 44.06 μs represents a smoothed REMPI spectrum of thermal atomic $Cl(^2P_{3/2})$ generated outside of the mass spectrometer.

(R = H, CH_3) and $ClONO_2$ photolysis experiments shall be presented in an upcoming contribution [44].

In the PF-TOF profiles displayed in Figs. 6 and 7, asterisks are experimental data points each one representing a channel reading of the digital recording unit. The dotted signals with a maximum around 44.06 μs in Figs. 6 and 7 correspond to smoothed TOF profiles of thermal Cl atoms which have been generated outside the mass spectrometer, transported into the ion source by the carrier gas and photoionized there. These dotted signals represent the imaging properties and the time resolution of our set-up. They serve as internal standard and as one of the tests to scrutinize the reliability of the present results. Further test studies for internal calibration included the registration of PF-TOF profiles of $Cl(^2P_{3/2})$ atoms generated in the Cl_2 photolysis at $\lambda = 308$ nm [45], in the ICl photolysis at $\lambda = 235$ nm [46], and in NOCl photolysis at $\lambda = 355$ nm (cf. Fig. 7). The product fine structure and non-adiabatic dissociation dynamics of this latter molecule has very recently been extensively investigated by Cao et al. [42]. Thus the comparison of our PF-TOF data with those presented in Ref. [42] which have been obtained under otherwise identical conditions, but with a linear TOF depicts a crucial test case for the performance of the ion optics with Reflectron incorporated in our mass spectrometer. In Fig. 7 are presented our experimental data for $Cl(^2P_{3/2})$ by asteriks and compared with the peak shape as reported in [42] which

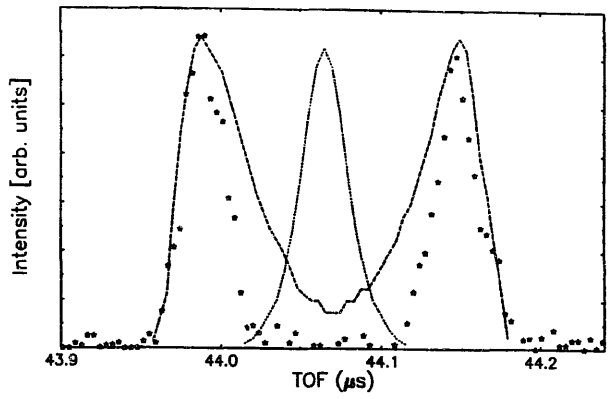

Fig. 7. REMPI PF-TOF profiles of $Cl(^2P_{3/2})$ generated in the photolysis of NOCl at $\lambda = 355$ nm. Asterisks represent experimental data points from the present investigation. The dashed profile is reproduced from Ref. [42]. For comparison the distribution reported in [42] was normalized to show the same splitting as in the present investigation. The dotted signal is due to Cl atoms generated outside of the mass spectrometer (cf. Fig. 6).

has been scanned-in from the publication. For the comparison the published data were normalized to show the same splitting as the present result.

Three findings can immediately be extracted from this comparison: (i) Due to the high mass resolution of the present spectrometer and a time resolution equivalent 5 ns per channel, only a much smaller number of data points becomes available to characterize each profile, as compared to the results of [42]. (ii) The TOF profiles of Cl atoms in thermal equilibrium with the carrier gas appear to possess a virtually identical shape as the photogenerated Cl atoms, the latter being only displaced by their forward/backward recoil energy. (iii) There is acceptable agreement between the profile shapes reported in [42] and the present results close to threshold. Discrepancies are apparent in the range where the convoluting angular distribution functions of Eq. (3) in Ref. [42] are most effective. Trajectory calculations were carried out to rationalize the apparent sharpening of the profiles [44]. It can be shown by computer simulation of ion trajectories, that the electric field conditions in the source used for determinations of recoil velocities can be made responsible for this distribution sharpening [44].

The experimental data for the Cl^+-signal splitting allow the calculation of the recoil energy deposited in the photofragment Cl as excess kinetic energy. The evaluation was based on relating reported recoil energy data for Cl atoms as determined by others in the photolysis of Cl_2 [45], in the photolysis of ICl [46] and of NOCl [42] to the experimental findings of the TOF analysis presented here. Computer simulation of ion trajectories also provided evidence [44] that—as expected—the magnitude of the observed Cl-ion signal splitting is related to the recoil energy of the photogenerated Cl-atoms through a single physical model, valid for all Cl-compounds studied.

The calculated data for the kinetic energy of photogenerated $Cl(^2P_{3/2})$ atoms from CH_3OCl as well as from HOCl photolysed at $\lambda = 308$ nm and at $\lambda = 235$ nm, respectively, are given in Table 3. The table also lists the respective data

Table 3
Kinetic energies in eV on the photofragments $Cl(^2P_{3/2})$ and $Cl(^2P_{1/2})$ in the photolysis of CH_3OCl and HOCl at different wavelengths

		CH_3OCl		HOCl	
$Cl(^2P_{3/2})$	Photolysis wavelength	$\lambda = 308$ nm	$\lambda = 235$ nm	$\lambda = 308$ nm	$\lambda = 235$ nm
	Splitting Δt (ns)	190 ± 10	240 ± 10	175 ± 10	195 ± 10
	Kinetic energy (eV)	0.81 ± 0.10	1.29 ± 0.10	0.69 ± 0.10	0.87 ± 0.10
$Cl^*(^2P_{1/2})$	Photolysis wavelength	$\lambda = 308$ nm	$\lambda = 238$ nm	$\lambda = 308$ nm	$\lambda = 238$ nm
	Splitting Δt (ns)	185 ± 10	230 ± 10	170 ± 10	190 ± 10
	Kinetic energy (eV)	0.77 ± 0.10	1.18 ± 0.10	0.64 ± 0.10	0.81 ± 0.10

for Cl atoms generated in the state $^2P_{1/2}$. The experimental error of $\Delta t = \pm 10$ ns given corresponds to an uncertainty of ± 2 channels from averaging readings from the transient recorder. This error transforms into an uncertainty of $\Delta E = 0.10$ V in kinetic energy. This is nearly as large as the energy difference $\Delta E(^2P_{1/2} - {}^2P_{3/2}) = 883\ cm^{-1}$ [47]. It is gratifying to note, however, that in all cases a slightly lower value for the kinetic energy is obtained for $Cl(^2P_{1/2})$ atoms.

4. Discussion

This paper concentrates on experimental investigations of the CH_3OCl photolysis and its dynamics. Equivalent results obtained in simultaneously performed investigations with HOCl are included at each stage to examine and/or to stress existing analogies. Since HOCl has been subject to several photochemical studies before [17–20,32] the results reported for this triatomic molecule can be utilized for comparisons with the present data for CH_3OCl. In addition, for HOCl theoretical studies have become available which cover several aspects of the photodissociation dynamics [15,16,34,48], thus offering quantum chemical support to interpretations based on experimental findings. Virtually none of these aspects have been covered in literature for CH_3OCl experimentally or theoretically. Thus the experimental results presented here for the first time seek support "by analogy". Three points shall briefly be considered:

(i) The ab initio data obtained for HOCl show that the lowest singlet excited states of this molecule are all strongly repulsive in the O-Cl coordinate [16]. By analogy and based on the high similarity of their electronic absorptions spectra [12] it is suggested that this situation equally prevails for CH_3OCl. Thus the photodissociation process for this simple alkyl hypochlorite is expected to be direct and fast. This has been corroborated experimentally by Thelen et al. [21] for the photodissociation of *tert*-butyl hypochlorite in which process the photofragment anisotropy parameter was found to be $\beta = 1.9 \pm 0.1$, implying a direct dissociation mechanism. From an analysis of the velocity distribution in REMPI PF-TOF profiles for the $Cl(^2P_{3/2})$ fragment in the present investigation further support is obtained, that in the photolysis of CH_3OCl as well as of HOCl channel (Eq. (a)) is the predominant, if not the exclusive dissociation channel. These findings are fully supported by the results of quantum yield determinations. Using molecular chlorine as actinometer, the total quantum yield for formation of $Cl(^2P_j)$ according to Eq. (a) was determined to be virtually unity for both hypochlorites. Formation of other products, i.e. Eqs. (b)–(d) were excluded to $< 10^{-2}$.

(ii) In a recently published model calculation on the photolysis of HOCl via the $1^1A''$ state, Offer and Balint-Kurti [48] predicted some correlation between OH and Cl spin-orbit states. Also correlations were made with predicted quantum state distributions resulting from photodissociation of HOCl via its $2^1A'$ state. Whereas the authors calculated no strong preference for either OH spin-orbit state in the photolysis at $\lambda = 306$ nm, dissociation via the $2^1A'$ should lead to preferred formation of $^2\Pi_{3/2}$ (F1 state). The present study, however, seems to indicate that in the photolysis at 308 nm and at 235 nm an inversion occurs in the spin-orbit population, with the $^2\Pi_{1/2}$ state being preferred if photolysis occurs via state $2^1A'$. However the limited resolution available in the present experiments does not permit a quantitative evaluation.

In disagreement with the prediction based on model calculations [48] on the correlation between OH and Cl spin-orbit states, in the present study an increase is noted in the population of the $Cl^*(^2P_{1/2})$ state in the photolysis at the shorter wavelengths. Whereas the increase in $OH(^2\Pi_{1/2})$ formation in the $2^1A' \leftarrow \tilde{X}^1A'$ transition as compared to $1^1A'' \leftarrow \tilde{X}^1A'$ is only tentatively suggested, the increase in $Cl^*(^2P_{1/2})$ population is firmly established (cf. Table 2). Thus it appears that a correlation exists, but it seems that the energetically higher spin-orbit state is preferentially formed at higher photon energies. More experimental work on HOCl photolysis and new theoretical investigations for the CH_3OCl photodissociation appear needed to remove this discrepancy.

(iii) The ensemble of molecules entering the mass spectrometer through the pulsed inlet valve, i.e. the hypoclorite molecules seeded in the carrier gas, will exhibit a velocity spread characterized by a Maxwellian velocity distribution. A rough estimate of the temperature decrease due to adiabatic expansion shows that, depending on inlet pressure, $T <$ 100 K should be accepted for the ensemble entering the ion source.

The photodissociation process gives rise to two radical species, as given by Eq. (3), each with its own internal energy and its own spread of recoil velocities. These quantities are correlated by the requirement Eq. (III)

$E_{photon} + E_{HOCl}$

$$\rightarrow D_O(HO\cdots Cl) + E_{trans} + E_{intOH} + E_{intCl} \quad (III)$$

At this point E_{trans} shall be considered only: The halogen fragments formed possess an anisotropic distribution of recoil velocities. This anisotropy results from the fact that the probability of an electric dipole allowed excitation process is proportional to $|\mu \cdot \epsilon|^2$, with μ being the transition dipole moment in the parent molecule and $\epsilon = \epsilon_{phot}$ the electric vector of the linearly polarized photolysis laser radiation. Thus the incident radiation interacts selectively with molecules for which μ happens to be parallel to ϵ_{phot}. Consequently the photoexcited parent molecule will be aligned in the laboratory frame with a distribution proportional to $\cos^2\theta$, where θ describes the angle between μ and ϵ_{phot}. For a direct photodissotiation process this alignment must be reflected in an anisotropic distribution of recoil fragments as given by the expression Eq. (a). In the present experiments the anisotropy parameter β was not determined. However, from the observed experimental splittings given in Δt/ns for $Cl(^2P_{3/2})$ as well as for $Cl^*(^2P_{1/2})$ atoms generated in the photolysis of CH_3OCl and HOCl, both photolyzed at $\lambda = 308$ nm and $\lambda = 235$ nm or 238 nm, respectively, the recoil kinetic energies are evaluated. Further experimental work is in progress to establish correlations.

5. Conclusions and atmospheric implications

Experimental evidence is presented in this contribution for the first time that photolysis of CH_3OCl at $\lambda = 308$ nm yields Cl-atoms with unity quantum yield. Thus CH_3OCl should be considered as atmospheric Cl-reservoir in the same way as HOCl is, for which a photolytic Cl-atom quantum yield of $\phi = 1.0$ at $\lambda = 308$ nm has been determined again. It has also been shown that other energetically possible channels, like formation of CH_3, HCl, ClO or O-atoms are to be excluded to $< 10^{-2}$. The relative spin-orbit state distribution of the photofragments varied strongly with photolysis wavelength. The probability for the generation of photofragments in the energetically higher spin-orbit state increased with photon energy, i.e. with light induced transitions into the 1′A″ and the 2′A′ states, respectively.

Whereas formation of photofragments in different spin-orbit states or with different rotational distributions, e.g. for OH radicals, may not have an implication on atmospheric chemistry, it is suggested that the formation of photofragments with high kinetic energies will be of relevance to the discussion of heterogeneous photoprocesses in the atmosphere. If the photolysis occurs in the gas phase, the translational energy of the fragment Cl-atoms will be dissipated in a few collisions with the atmospheric main constituents N_2 and O_2. If, however, molecules adsorbed at or incorporated into aerosol particles are photolyzed, the first encounters of the kinetically hot photofragment will be with matrix material, i.e. predominantly with H_2O or with organic/inorganic species depending on aerosol composition. In most cases the hot halogen atom will abstract an H-atom and thus heterogeneous photolysis of the oxychloride may be considered as source for atmospheric HCl. No estimates can be given on the strength of this source since at present no estimates are available on the importance of heterogeneous photo processes in the atmosphere.

Acknowledgements

The work described in this contribution was supported by the BMFT, Bonn, and by the European Commission within their Environmental Programs. U.K. acknowledges a "Promotions Stipendium des Landes Schleswig-Holstein".

Appendix

Photofragmentation/photoionization (PF/PI) occurred in a region of the ion source which consisted of a cup-shaped repeller electrode, kept at a bias voltage of +705 V, and a conical extraction electrode the potential of which was varied to reach estimated field strengths in the PF/PI-region in the range $90\ V\ cm^{-1} \leq E_{es} \leq 700\ V\ cm^{-1}$. Ions were extracted from this region by (two) plates kept at ground potential and had to traverse the ion lens system before entering the field free flight tube, at the end of which a Reflectron was located. Extensive calculations were carried out for the whole system using SIMION software [51] simulating the dependence of ion trajectories on voltage settings, nascent energy of the photofragment and on the geometry of the Reflectron MS. In Fig. 8 are depicted calculated ion trajectories in the ion source region for the limiting conditions $E_{est} = 600\ V\ cm^{-1}$ (a) and $E_{est} = 100\ V\ cm^{-1}$ (b), both for an assumed recoil energy of the photogfragment ^{35}Cl atom of $E_{kin} = 2.5$ eV. This high

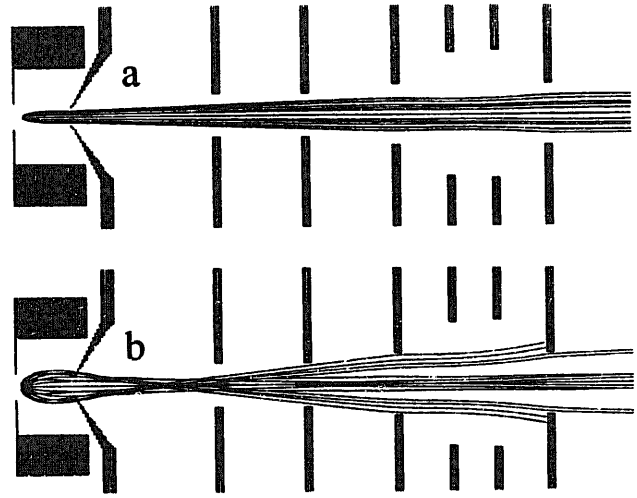

Fig. 8. Calculated ion trajectories for $^{35}Cl^+$ ions photogenerated in the ion source. The recoil energy was assumed to be $E_{kin} = 2.5$ eV. Field strength between cup-shaped repeller and conical extraction lens was set at (a) $600\ V\ cm^{-1}$ and (b) $100\ V\ cm^{-1}$.

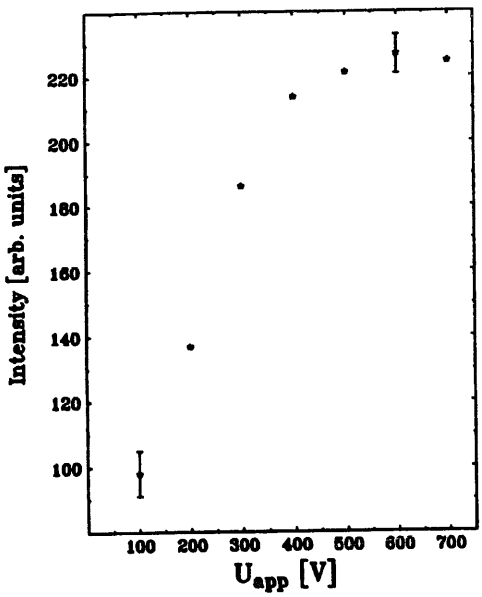

Fig. 9. Signal intensity changes for the photofragment ^{35}Cl as function of applied potential between repeller electrode and conical extraction lens (cf. Fig. 8). A plateau was reached for all systems studied.

recoil energy was chosen to clearly demonstrate the efficient ion collection at high field strength and the discrimination at low field strength occurring in the ion source.

The calculation demonstrated that for fields $E \geq 400$ V cm^{-1}, the ion source used is fully transparent for all photofragments generated with $E_{kin} \leq 2.5$ eV independent of the dynamics of the photodissociation process. At low field strengths the ion source is transparent only for fragments with recoil energy inside a characteristic solid angle of the TOF axis, but discriminates against fragments with strong velocity components perpendicular to the TOF axis. At low field strength, on the other side, the increased residence time of the photofragments in the PF/PI region resulted in the increased turn around time before the ions were accelerated down the flight tube. The measurement of Δt under these conditions permitted the determination of E_{kin} with good precision.

The results shown in Fig. 9 are considered to be an experimental verification of the conclusions drawn from the ion trajectory simulations. Increasing the potential applied to the conical extraction electrode from 100 V to 700 V, the PF ion intensity was more than doubled and reached a plateau around 500 V. Such a plateau was reached for all systems described, including the calibration gas Cl_2. At the same time the flight time and the time lag decreased (not shown). The two peaks nearly coalesced into one signal with a pronounced dip at the top. More details shall be presented elsewhere [44].

References

[1] B. Reimann, F. Kaufmann, J. Chem. Phys. 69 (1978) 2925.
[2] R.M. Stimpfle, R.A. Perry, C.J. Howard, J. Chem. Phys. 71 (1979) 5183.
[3] M.T. Leu, Geophys. Res. Lett. 7 (1980) 173.
[4] T.J. Leck, J.E.L. Cook, J.W. Birks, J. Chem. Phys. 72 (1980) 2364.
[5] F.C. Cattell, R.A. Cox, J. Chem. Soc. Faraday Trans. 82 (1986) 1413.
[6] C.A. Ennis, J.W. Birks, J. Phys. Chem. 92 (1988) 1119.
[7] F. Helleis, J.N. Crowley, G.K. Moortgat, J. Phys. Chem. 97 (1993) 11464 and Geophys. Res. Lett. 21 (1994) 1298.
[8] R.D. Kenner, K.R. Ryan, I.C. Plumb, Geophys. Res. Lett. 20 (1993) 1571.
[9] A.S. Kukui, T.P.W. Jungkamp, R.N. Schindler, Ber. Bunsenges. Phys. Chem. 98 (1994) 1298.
[10] P. Biggs, C.E. Canosa-Mas, J.M. Frachebout, D. Shallcross, R.P. Wayne, Geophys. Res. Lett. 22 (1995) 1221.
[11] R.P. Wayne, G. Poulet, P. Biggs, J.P. Burrows, R.A. Cox, P.J. Crutzen, G.D. Hayman, M.E. Jenkin, G. LeBras, G.K. Moortgat, U. Platt, R.N. Schindler, Atmos. Environ. 29 (1995) 2677.
[12] T.P.W. Jungkamp, U. Kirchner, M. Schmidt, R.N. Schindler, J. Photochem. and Photobiol. A, Chem. 91 (1995) 1.
[13] J.N. Crowley, F. Helleis, R. Müller, G.K. Moortgat, P.J. Crutzen, J.J. Orlando, J. Geophys. Res. 99 (1994) 20683.
[14] J.B. Burkholder, J. Geophys. Res. 98 (1993) 2963.
[15] S. Nanbu, S. Iwata, J. Phys. Chem. 96 (1992) 2103.
[16] H. Guo, J. Phys. Chem. 97 (1993) 2602.
[17] A.J. Bell, P.R. Pardon, C.G. Hickman, J.G. Frey, J. Chem. Soc. Faraday Trans. 86 (1990) 3831.
[18] C.G. Hickman, A. Brickell, J.G. Frey, Chem. Phys. Lett. 185 (1991) 101.
[19] C.G. Hickman, N. Shaw, M.J. Crawford, A.J. Bell, J.G. Frey, J. Chem. Soc. Faraday Trans. 89 (1993) 1623.
[20] A.J. Bell, S.A. Boggis, J.M. Dyke, J.G. Frey, R. Richter, N. Shaw, M. Tabrizchi, J. Chem. Soc. Faraday Trans. 90 (1994) 17.
[21] M.A. Thelen, P. Felder, J.G. Frey, J.R. Huber, J. Phys. Chem. 97 (1993) 6220.
[22] R. Vogt, R.N. Schindler, Ber. Bunsenges. Phys. Chem. 97 (1993) 819.
[23] T. Sandmeyer, Ber. Deutsche Chem. Ges. 19–I (1886) 857.
[24] S. Arepalli, N. Presser, D. Robie, R.J. Gordon, Chem. Phys. Lett. 118 (1985) 88.
[25] S. Bashkin, J.O. Stoner Jr., Atomic Energy-level and Grotian Diagram Vol. II, North Holland Publishing Comp., 1978.
[26] Th. Benter, Doctoral Thesis, Christian-Albrechts-Universität Kiel, 1993.
[27] J.W. Hudgens, T.G. DiGuiseppe, M.C. Lin, J. Chem. Phys. 79 (1983) 571.
[28] M. Collard, P. Kerwin, A. Hodgson, Chem. Phys. Lett. 179 (1991) 442.
[29] E. de Beer, M.P. Koopmans, C.A. de Lange, Y. Wang, W.A. Chupka, J. Chem. Phys. 94 (1991) 7634.
[30] G.H. Dieke, H.M. Crosswhite, J. Quant. Spectros. Radiat. Transfer 2 (1962) 97.
[31] M.H. Alexander, P. Andresen, R. Bacis, R. Bersohn, F.J. Comes, Gericke, E.R. Grant, B.J. Howard, J.R. Huber, D.S. King, J.L. Kinsey, K. Kleinermans, K. Kuchitsu, A.C. Luntz, A.J. McCafferty, B. Pouilly, H. Reisler, E.W. Rothe, M. Shapiro, J.P. Simoms, R. Vasudev, J.R. Wiesenfeld, C. Wittig, R.N. Zare, J. Chem. Phys. 89 (1988) 1749.
[32] R. Vogt, R.N. Schindler, J. Photochem. and Photobiol. A: Chem. 66 (1992) 133, and further references given therein.
[33] W.D. Anderson, M.C.L. Gerry, R.W. Davis, J. Mol. Spectrosc. 115 (1986) 117.
[34] A.R. Offer, G.G. Balint-Kurti, J. Phys. Chem. 101 (1994) 10 416.
[35] V.J. Barclay, B.A. Collings, J.C. Polanyi, J.H. Wang, J. Phys. Chem. 95 (1991) 2921.
[36] K. Tonokura, Y. Matsumi, M. Kawasaki, K. Tasaki, R. Bersohn, J. Chem. Phys. 97 (1992) 8210.
[37] E. Tiemann, H. Kanamori, E.J. Hirota, J. Chem. Phys. 88 (1988) 2457.
[38] Y. Matsumi, K. Tonokura, M. Kawasaki, J. Chem. Phys. 97 (1992) 1065.

[39] W.B. De More, S.P. Sander, D.M. Golden, R.F. Hampson, M.J. Kuryle, C.J. Howard, A.J. Ravishankera, C.E. Kolb, M.J. Molina, Chemical Kinetics and Photochemical Data for Use in Statospheric Modelling, JPL Publication 94–26.
[40] R.N. Zare, Mol. Photochem. 4 (1972) 1.
[41] S.M. Penn, C.C. Hayden, K.J. Carlson Muyskens, F.F. Crim, J. Chem. Phys. 89 (1988) 2909.
[42] J. Cao, Y. Wang, C.X.W. Quian, J. Chem. Phys. 103 (1995) 9653.
[43] M.N.R. Ashfold, I.R. Lambert, D.H. Mordaunt, G.P. Morley, C.M. Western, J. Phys. Chem. 96 (1992) 2938.
[44] S. Schmidt, Th Benter, R.N. Schindler, to be published.
[45] Y. Wang, H.-P. Loock, J. Cao, C.X.W. Qian, J. Chem. Phys. 102 (1995) 808.
[46] C.K. Ni, G.W. Flynn, Chem. Phys. Lett. 210 (1993) 333.
[47] J. Park, Y. Lee, G.W. Flynn, Chem. Phys. Lett. 186 (1991) 441.
[48] A.R. Offer, G.G. Balint-Kurti, Chem. Phys. Lett. 247 (1995) 173.
[49] E. Rühl, A. Jefferson, V. Vaida, J. Phys. Chem. 94 (1990) 2990.
[50] D.S. Green, G.A. Bickel, S.C. Wallace, J. Mol. Spectr. 150 (1991) 303.
[51] SIMION 3D version 6.0, Princeton Electronics Systems, Inc., Princeton, NJ, 1995.